

## **Improved Sensitivity, Low-cost Uncooled Infrared (IR) Detector Focal-plane Arrays-Year 3, Quarter 1**

**by Wendy L. Sarney, Kimberley A. Olver, John W. Little,  
Frank E. Livingston, Krisztian Niesz, and Daniel E. Morse**

**ARL-TR-5988**

**April 2012**

## **NOTICES**

### **Disclaimers**

The findings in this report are not to be construed as an official Department of the Army position unless so designated by other authorized documents.

Citation of manufacturer's or trade names does not constitute an official endorsement or approval of the use thereof.

Destroy this report when it is no longer needed. Do not return it to the originator.

# **Army Research Laboratory**

Adelphi, MD 20783-1197

---

---

**ARL-TR-5988**

**April 2012**

---

## **Improved Sensitivity, Low-cost Uncooled Infrared (IR) Detector Focal-plane Arrays-Year 3, Quarter 1**

**Wendy L. Sarney, Kimberley A. Olver, and John W. Little**  
**Sensors and Electron Devices Directorate, ARL**

**Frank E. Livingston**  
**The Aerospace Corporation**

**and**

**Krisztian Niesz and Daniel E. Morse**  
**Institute for Collaborative Biotechnologies**  
**University of California Santa Barbara**

REPORT DOCUMENTATION PAGE			Form Approved OMB No. 0704-0188		
<p>Public reporting burden for this collection of information is estimated to average 1 hour per response, including the time for reviewing instructions, searching existing data sources, gathering and maintaining the data needed, and completing and reviewing the collection information. Send comments regarding this burden estimate or any other aspect of this collection of information, including suggestions for reducing the burden, to Department of Defense, Washington Headquarters Services, Directorate for Information Operations and Reports (0704-0188), 1215 Jefferson Davis Highway, Suite 1204, Arlington, VA 22202-4302. Respondents should be aware that notwithstanding any other provision of law, no person shall be subject to any penalty for failing to comply with a collection of information if it does not display a currently valid OMB control number.</p> <p><b>PLEASE DO NOT RETURN YOUR FORM TO THE ABOVE ADDRESS.</b></p>					
1. REPORT DATE (DD-MM-YYYY) April 2012		2. REPORT TYPE Final		3. DATES COVERED (From - To) May to August 2010	
4. TITLE AND SUBTITLE Improved Sensitivity, Low-cost Uncooled Infrared (IR) Detector Focal-plane Arrays-Year 3, Quarter 1			5a. CONTRACT NUMBER		
			5b. GRANT NUMBER		
			5c. PROGRAM ELEMENT NUMBER		
6. AUTHOR(S) Wendy L. Sarney, Kimberley A. Olver, John W. Little, Frank E. Livingston, Krisztian Niesz, and Daniel E. Morse			5d. PROJECT NUMBER		
			5e. TASK NUMBER		
			5f. WORK UNIT NUMBER		
7. PERFORMING ORGANIZATION NAME(S) AND ADDRESS(ES) U.S. Army Research Laboratory ATTN: RDRL-SEE-I 2800 Powder Mill Road Adelphi, MD 20783-1197			8. PERFORMING ORGANIZATION REPORT NUMBER  ARL-TR-5988		
9. SPONSORING/MONITORING AGENCY NAME(S) AND ADDRESS(ES) Army Research Office Institute Collaborative Biotechnology Santa Barbara CA 93106-5100			10. SPONSOR/MONITOR'S ACRONYM(S)		
			11. SPONSOR/MONITOR'S REPORT NUMBER(S)		
12. DISTRIBUTION/AVAILABILITY STATEMENT Approved for public release; distribution unlimited.					
13. SUPPLEMENTARY NOTES					
14. ABSTRACT <p>In this report, our attention is focused on the fabrication, laser processing, and electrical testing of integrated prototype infrared (IR)-device heterostructures. The program goals correspond to the continued expansion of our barium titanate (<math>\text{BaTiO}_3</math>) and barium strontium titanate (<math>\text{Ba}_{1-x}\text{Sr}_x\text{TiO}_3</math>) nanomaterial synthesis capabilities and deposition methods; laser-induced pyroelectric phase conversion studies and nanoscale characterization of the pyroelectric activation process; and fabrication and electrical testing of standardized IR heterostructures.</p>					
15. SUBJECT TERMS Infrared, perovskites					
16. SECURITY CLASSIFICATION OF:			17. LIMITATION OF ABSTRACT  UU	18. NUMBER OF PAGES  24	19a. NAME OF RESPONSIBLE PERSON Wendy L. Sarney
a. REPORT Unclassified	b. ABSTRACT Unclassified	c. THIS PAGE Unclassified			19b. TELEPHONE NUMBER (Include area code) (301) 394-5761

---

## Contents

---

<b>List of Figures</b>	<b>iv</b>
<b>Acknowledgments</b>	<b>v</b>
<b>1. Introduction</b>	<b>1</b>
<b>2. Progress by the Aerospace Corporation (Aerospace)</b>	<b>3</b>
2.1 Laser-scripted Direct-write Processing of BaTiO <sub>3</sub> and BaSrTiO <sub>3</sub> Thin-films for Electrical Analysis.....	3
2.2 Influence of Laser Processing on Perovskite Thin-film Morphology .....	4
<b>3. Progress by the Institute for Collaborative Biotechnologies (ICB)</b>	<b>6</b>
3.1 Electrophoretic Deposition of Ba <sub>1-x</sub> Sr <sub>x</sub> TiO <sub>3</sub> Nanoparticles: A New Approach to High Quality Perovskite Films .....	6
<b>4. Progress by the Army Research Laboratory (ARL)</b>	<b>8</b>
4.1 Electrical Characterization of Perovskite Films; Refinement of Metallization Protocol; Ba <sub>1-x</sub> Sr <sub>x</sub> TiO <sub>3</sub> Film Hybridization .....	8
<b>5. Plans and Goals for Year 3, Quarter 2</b>	<b>12</b>
<b>List of Symbols, Abbreviations, and Acronyms</b>	<b>13</b>
<b>Distribution List</b>	<b>15</b>

---

## List of Figures

---

Figure 1. Project schedule.....	2
Figure 2. (a) Low and (b) high magnification photomicrographs acquired following the laser-scripted pixelation and pyroelectric activation of 4x4-(8x8) arrays on a pure, undoped BaTiO <sub>3</sub> thin-film at $\lambda=355$ nm. The inset (upper right) shows a single 100 $\mu\text{m}$ x 100 $\mu\text{m}$ pixel element. ....	3
Figure 3. RMS surface roughness measured as a function of total exposure dose for BaTiO <sub>3</sub> films following laser-scripted processing at $\lambda = 355$ nm. The RMS roughness values were acquired during AFM/PFM contact mode scanning and correspond to image regions with dimensions of 10 $\mu\text{m}$ x 8 $\mu\text{m}$ . The fit (solid black curve) is intended as a visual guide. ....	5
Figure 4. PFM images (in-plane polarization) of a BaTiO <sub>3</sub> film that were acquired (a) prior to laser exposure and (b) following laser-scripted patterning and pyroelectric phase conversion at $\lambda = 355$ nm. The ferroelectric regions are highly homogeneous with domains sizes exceeding 1 $\mu\text{m}$ . The image sizes are 5 $\mu\text{m}$ x 5 $\mu\text{m}$ . ....	6
Figure 5. Schematic representation of electrophoretic deposition to fabricate Ba <sub>1-x</sub> Sr <sub>x</sub> TiO <sub>3</sub> films. ....	7
Figure 6. SEM images of films of Ba <sub>1-x</sub> Sr <sub>x</sub> TiO <sub>3</sub> titanate nanoparticles deposited through electrophoretic deposition (EPD). ....	8
Figure 7. Ba <sub>1-x</sub> Sr <sub>x</sub> TiO <sub>3</sub> thin-film following metallization and wire bonding. ....	9
Figure 8. High magnification image of wirebond- Ba <sub>1-x</sub> Sr <sub>x</sub> TiO <sub>3</sub> film interface.....	10
Figure 9. Optimized Ba <sub>1-x</sub> Sr <sub>x</sub> TiO <sub>3</sub> thin-film following metallization and prior to hybridization. ....	11
Figure 10. Hybridized Ba <sub>1-x</sub> Sr <sub>x</sub> TiO <sub>3</sub> thin-film sample that has been pulled apart to verify proper indium bump contact. Images correspond to the film (left) and fanout chip (right). ..	12

---

## **Acknowledgments**

---

We acknowledge support by the Institute for Collaborative Biotechnologies through grant DAAD19-03-D-0004 from the U.S. Army Research Office and The Aerospace Corporation Independent Research and Development (IR&D) Program and the Product and Development Program (PDP).

INTENTIONALLY LEFT BLANK.



---

## 1. Introduction

---

This proposal offers a revolutionary approach for the design and fabrication of passive uncooled infrared (IR) focal-plane array (FPA) detectors that retain improved sensitivity, low weight and power consumption, and fast response times, along with low-cost rapid prototype manufacture compatibility. The project objectives are ambitious and correspond to the fabrication of precision micro- and nanoscale patterned two-dimensional (2-D) FPAs of perovskite-based materials for integration with the diverse and rapidly evolving number of Army devices requiring uncooled IR detectors, such as Soldiers' driver vision enhancement (DVE), rifle sights, seeker munitions and target acquisition, unattended ground sensors (UGSs), unmanned ground vehicles (UGVs), and unattended aerial vehicles (UAVs).

The success of this program relies upon the rapid growth and continued development of several key research areas: new nanostructured materials synthesis, laser material processing techniques, and microelectromechanical system (MEMS) detection device fabrication and testing.

Accordingly, our approach involves a three-way close collaboration between The Aerospace Corporation, The Institute for Collaborative Biotechnologies (ICB), and the U.S. Army Research Laboratory (ARL). The Aerospace Corporation's patented direct-write digitally scripted laser processing technique will be used in conjunction with the ICB's bio-inspired, kinetically controlled low-temperature synthesis of pyroelectric perovskite nanoparticles to fabricate patterned 2-D FPAs. Close integration with ARL's expertise in IR technology will ensure fabrication, performance testing, and optimization of device architectures tailored to Army needs, and facilitate a process that is compatible with ultimate monolithic incorporation into commercial readout integrated circuits (ROICs).

As we begin the third and final year of this 6.2 applied research program, our attention is focused on the fabrication, laser processing, and electrical testing of integrated prototype IR- device heterostructures. The project schedule is outlined in figure 1. The program goals for year 3-quarter 1 (Y3Q1) corresponded to the continued expansion of our barium titanate ( $\text{BaTiO}_3$ ) and barium strontium titanate ( $\text{Ba}_{1-x}\text{Sr}_x\text{TiO}_3$ ) nanomaterial synthesis capabilities and deposition methods, laser-induced pyroelectric phase conversion studies and nanoscale characterization of the pyroelectric activation process, and fabrication and electrical testing of standardized IR heterostructures. Respective team highlights include:

- *Aerospace*: Conducted laser-scripted pixelation and pyroelectric activation of 8x8 pixel sub- arrays and 4x4-(8x8) pixel master arrays on  $\text{BaTiO}_3$  and  $\text{Ba}_{1-x}\text{Sr}_x\text{TiO}_3$  thin-film test structures for electrical characterization by ARL. These studies included the laser processing of perovskite thin films prepared by complementary low temperature synthesis techniques—kinetically controlled vapor diffusion catalytic synthesis (ICB) and metal-organic solution deposition (ARL). Efforts also focused on the nanoscale topographic and

ferroelectric analysis of the films pre- and post-laser processing. Atomic force microscopy (AFM) and newly developed piezoresponse force microscopy (PFM) capabilities were used to study the relationship between the laser processing conditions and the physical properties of the pyroelectrically activated thin-films.

- *ICB*: Extended the bio-inspired vapor diffusion catalytic methods to include the electrophoretic deposition (EPD) of  $\text{Ba}_{1-x}\text{Sr}_x\text{TiO}_3$  nanoparticles. This new deposition approach offers an important pathway for the fabrication of perovskite films with improved electrical and mechanical properties along with increased density and uniformity.
- *ARL*: Continued with the testing of a newly constructed electrical measurement system for capacitance and conductance measurements on perovskite thin-film heterostructures, and further developed the protocol for thin-film metallization and wire bonding. Efforts also focused on the optimization of  $\text{Ba}_{1-x}\text{Sr}_x\text{TiO}_3$  thin-film deposition for proper electrical isolation, and hybridization of the thin film to a fanout chip was achieved.

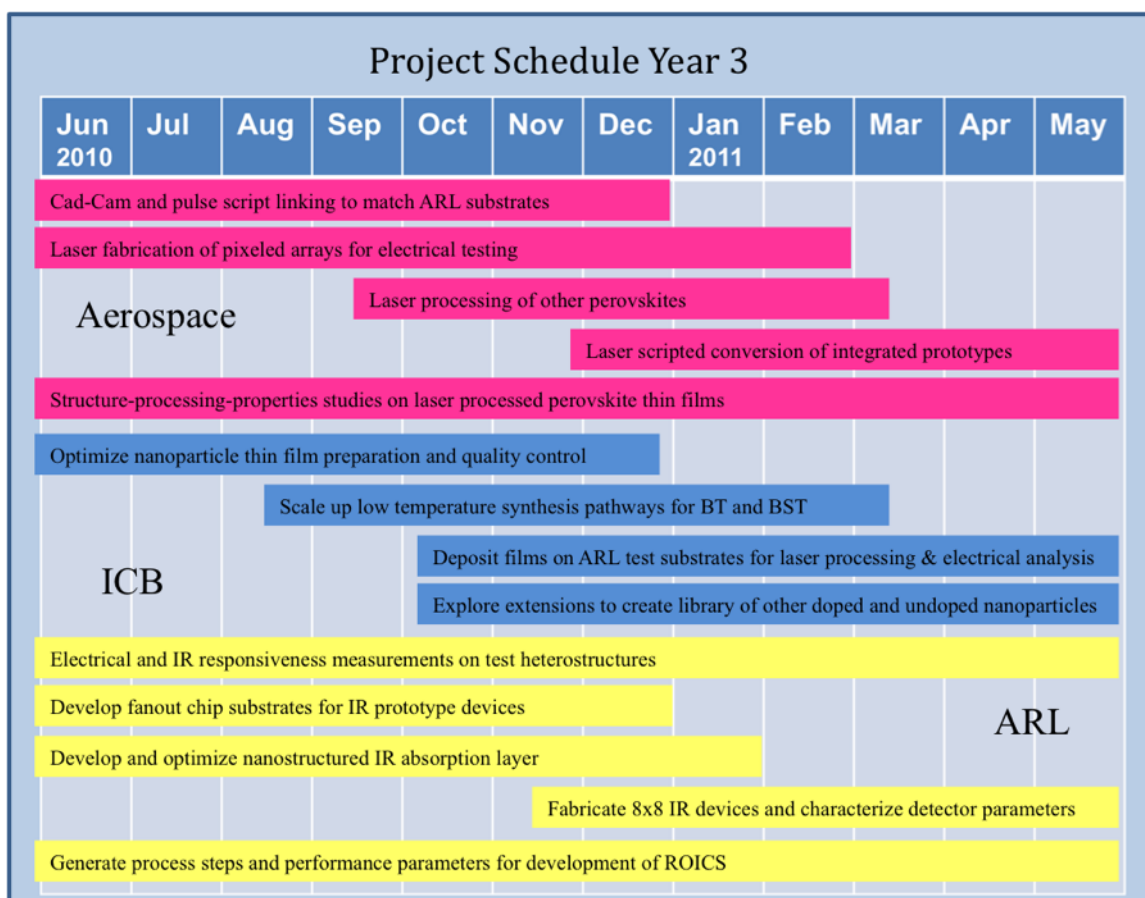


Figure 1. Project schedule.

All project teams have accomplished their respective planned milestones for Y3Q1 with distinction, and highlights of the major activities are provided in the following sections.

---

## 2. Progress by the Aerospace Corporation (Aerospace)

---

### 2.1 Laser-scripted Direct-write Processing of BaTiO<sub>3</sub> and BaSrTiO<sub>3</sub> Thin-films for Electrical Analysis

During this quarter, digitally scripted laser genotype processing techniques were implemented to create patterned and pyroelectrically active pixel arrays on undoped and cerium oxide (CeO<sub>2</sub>) doped BaTiO<sub>3</sub> and Ba<sub>1-x</sub>Sr<sub>x</sub>TiO<sub>3</sub> thin films deposited on titanium platinum on silicon (TiPt:Si) substrates. The perovskite thin films were prepared by complementary low temperature synthesis techniques—kinetically controlled vapor diffusion catalytic synthesis and metal-organic solution deposition (MOSD)—which produced high quality, crack-free homogeneous thin films and promote benign material processing conditions compatible with ultimate monolithic integration with commercial ROIC.

Laser-scripted direct-write pulse modulation was used to convert pixelated regions (100 x 100  $\mu\text{m}$ ) of the perovskite thin films from the pyroelectrically inactive cubic polymorph to the pyroelectrically active tetragonal polymorph. Figure 2 shows photomicrographs of an undoped BaTiO<sub>3</sub> thin-film sample (KN011210 TiPt) following laser pixelation and pyroelectric phase activation at  $\lambda = 355 \text{ nm}$  (80 MHz, 10 ps full width at half maximum [FWHM]). The BaTiO<sub>3</sub>:TiPt:Si sample was 10 mm x 10 mm in size with a thickness in excess of 1  $\mu\text{m}$ , and contained sixteen 8x8 pixel sub-arrays for a total of 1024 laser-pixelated regions. The single 8x8 sub-array patterns comprise 64 individual pixels, where the pixel dimensions are 100  $\mu\text{m}$  x 100  $\mu\text{m}$  with a lateral spacing of 100  $\mu\text{m}$  and a center-to-center spacing of 200  $\mu\text{m}$ . The pixel array dimensions were selected to match the ARL mask geometries for metal contact deposition.

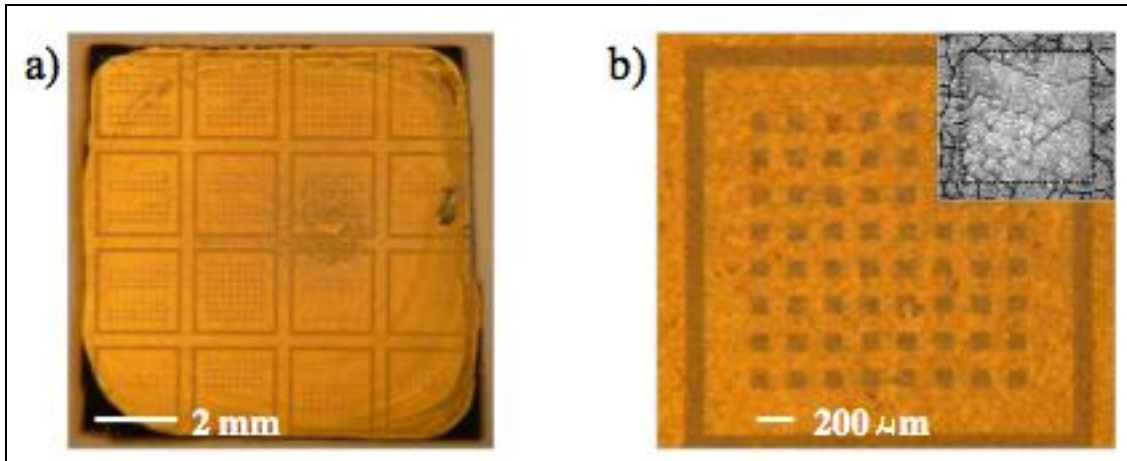


Figure 2. (a) Low and (b) high magnification photomicrographs acquired following the laser-scripted pixelation and pyroelectric activation of 4x4-(8x8) arrays on a pure, undoped BaTiO<sub>3</sub> thin-film at  $\lambda = 355 \text{ nm}$ . The inset (upper right) shows a single 100  $\mu\text{m}$  x 100  $\mu\text{m}$  pixel element.

Each pixel shown in figure 2 is laser patterned using a sequential line fill with a lateral step-over that is comparable to the laser spot size (1–3  $\mu\text{m}$  diameter typical). Equivalent laser processing parameters—in the form of laser pulse “scripts” that are “linked” on a per spot basis to the tool path geometry in Cartesian space and contain specific information on laser pulse energy, polarization, wavelength, etc.—are applied to a series of four pixels so that 16 sets of laser processing parameters or “scripts” are administered to each 64-pixel set. The large laser processing parameter set will help to optimize the pyroelectric phase activation protocol and facilitate the correlation of the laser processing conditions with the electrical properties of the pixel domains. Additionally, this laser-scripted redundancy can be implemented to assess the reproducibility of pyroelectric phase activation and film homogeneity across the entire spin-cast perovskite sample. The variation in pixel contrast uniformity and darkness revealed in figure 1 arise from the diverse set of laser processing pulse scripts that were implemented for patterning and do not correspond to inhomogeneities or variegations in the perovskite thin film.

Additional sets of laser-pixelated  $\text{BaTiO}_3\text{:TiPt:Si}$  and  $\text{Ba}_{1-x}\text{Ti}_x\text{O}_3\text{:TiPt:Si}$  samples have been shipped to ARL, and electrical analysis and pyroelectrical responsiveness tests are continuing.

## 2.2 Influence of Laser Processing on Perovskite Thin-film Morphology

Our Y3Q1 efforts have also focused on the effect of the laser processing conditions on the physical properties of the bio-inspired perovskite thin films. Through these studies we are attempting to elucidate the complex interplay between multiple laser processing parameters—such as pulse “script” profile, pulse repetition rate, pulse length, per-pulse fluence, and total exposure dose—and seeking to optimize the electrical properties and pyroelectric response of the laser-processed perovskite thin films. As discussed in our previous quarterly reports, we have successfully developed and applied PFM techniques for nanoscale characterization of the structural and ferroelectric properties of laser-processed barium titanate and barium strontium titanate thin films. Contact scanning mode PFM has been implemented to simultaneously measure surface profile variations and topography combined with the piezoresponse and ferroelectric phase contrast.

Figure 3 displays the surface roughness as a function of total exposure dose and corresponds to the laser-scripted processing of a  $\text{BaTiO}_3$  film (thickness  $>2\ \mu\text{m}$ ) at  $\lambda = 355\ \text{nm}$  (80 MHz, 10 ps). A single laser pulse “script” profile was used for all measurements shown in figure 3. The total exposure dose accounts for the per-pulse fluence and number of pulses that were delivered to each laser spot and thus represents the total integrated energy deposited per unit area.

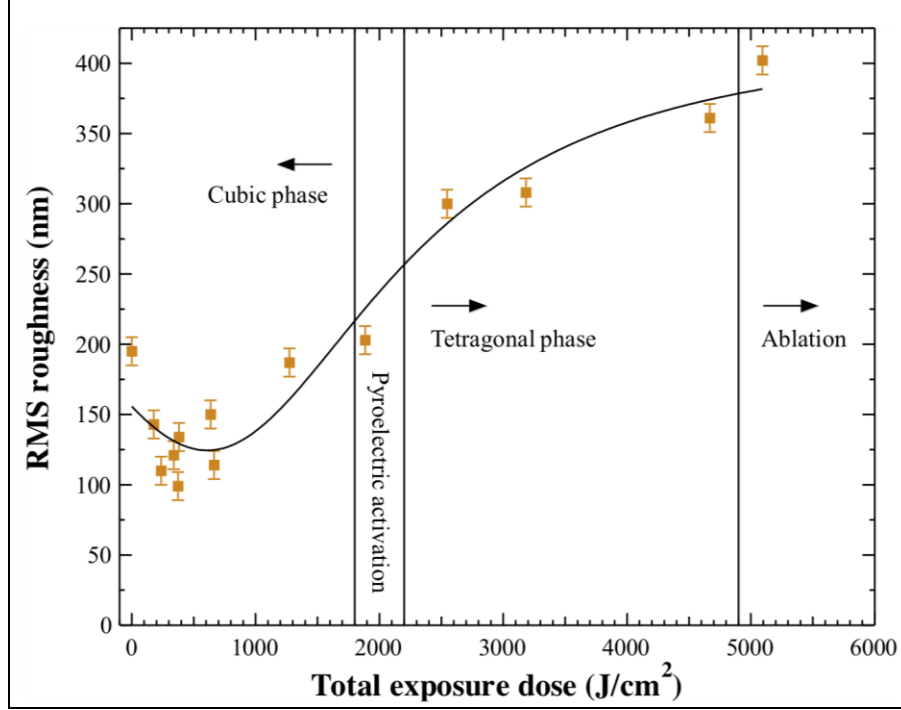


Figure 3. RMS surface roughness measured as a function of total exposure dose for BaTiO<sub>3</sub> films following laser-scripted processing at  $\lambda = 355$  nm. The RMS roughness values were acquired during AFM/PFM contact mode scanning and correspond to image regions with dimensions of  $10\ \mu\text{m} \times 8\ \mu\text{m}$ . The fit (solid black curve) is intended as a visual guide.

Several trends and features are noteworthy:

1. The cubic-to-tetragonal phase conversion is accomplished at laser exposure doses of  $\sim 1800\text{--}2200\ \text{J/cm}^2$ , where the pyroelectric activation of the film was confirmed via post-processing PFM analysis (figure 4);
2. The surface roughness of the perovskite film is significantly reduced under low fluence and low dose conditions, which suggests appreciable smoothing, compaction and densification of the BaTiO<sub>3</sub> film;
3. The surface roughness of the laser-processed film is comparable to the surface roughness of the native (as-received) film near the phase conversion threshold and again reveals that laser-scripted processing facilitates pyroelectric phase conversion with minimal disruption to the perovskite film; and
4. Ablation and delamination of the BaTiO<sub>3</sub> film occurs at total exposure doses that exceed  $\sim 4800\ \text{J/cm}^2$ .

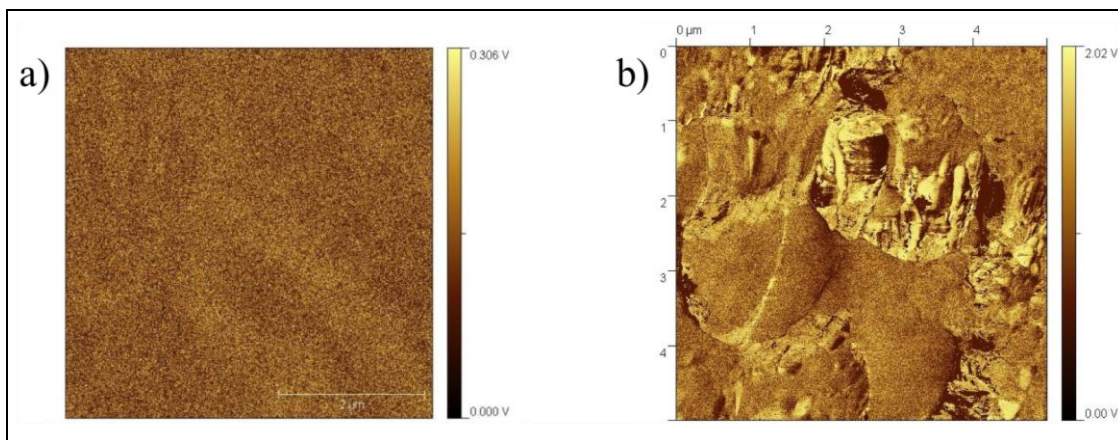


Figure 4. PFM images (in-plane polarization) of a  $\text{BaTiO}_3$  film that were acquired (a) prior to laser exposure and (b) following laser-scripted patterning and pyroelectric phase conversion at  $\lambda = 355$  nm. The ferroelectric regions are highly homogeneous with domains sizes exceeding  $1\ \mu\text{m}$ . The image sizes are  $5\ \mu\text{m} \times 5\ \mu\text{m}$ .

Based on these results, we are now exploring the capability of using laser-scripted processing for annealing the perovskite films prior to laser-pixelation and pyroelectric activation. Our aim is to induce additional compaction and densification of the nascent films and thereby enhance the films' homogeneity and electrical properties.

Figure 4a shows a PFM image of a  $\text{BaTiO}_3$  film sample that was acquired prior to laser-scripted exposure at  $\lambda = 355$  nm and, as anticipated, shows no in-plane (polarization parallel to sample surface) piezoresponse or ferroelectric phase contrast for the as-received cubic crystalline  $\text{BaTiO}_3$  film. Following laser-scripted exposure at  $\lambda = 355$  nm ( $\sim 1 \times 10^6$  pulses, per-pulse fluence  $= 2.0\ \text{mJ} \cdot \text{cm}^{-2}$ ), the PFM results in figure 3b reveal appreciable ferroelectric phase contrast and confirm successful pyroelectric conversion to the tetragonal phase.

We are continuing to implement and refine our PFM techniques to extract important phase contrast and electrical property data for the laser-processed and nanostructured perovskite films.

---

### 3. Progress by the Institute for Collaborative Biotechnologies (ICB)

---

#### 3.1 Electrophoretic Deposition of $\text{Ba}_{1-x}\text{Sr}_x\text{TiO}_3$ Nanoparticles: A New Approach to High Quality Perovskite Films

Because previous results at Aerospace showed fragility of our thin  $\text{BaTiO}_3$  film prepared by layer-by-layer spin-casting, and because electrical shorting of those films observed at ARL suggested the presence of voids and variations in density, we have begun to explore electrophoretic deposition of our  $\text{BaTiO}_3$  nanoparticles to fabricate thicker, more uniformly dense, and more robust films. In this method, a DC voltage is applied to electrodes immersed in a colloidal suspension containing the nanoparticles to be deposited (figure 5). A solvent mixture of

methoxyethanol/acetylacetone (AcAc) is used to impart a positive charge to the nanoparticles and maintain their dispersion through electrostatic repulsion. This dispersion should reduce aggregation, improving the uniform density of the resulting films produced by EPD of the charged single particles. We presently are optimizing particle concentration, deposition time and applied voltage, starting with concentrations ranging from 3 to 30 g/L, voltages from 1 to 150 V, and deposition times from seconds to minutes.

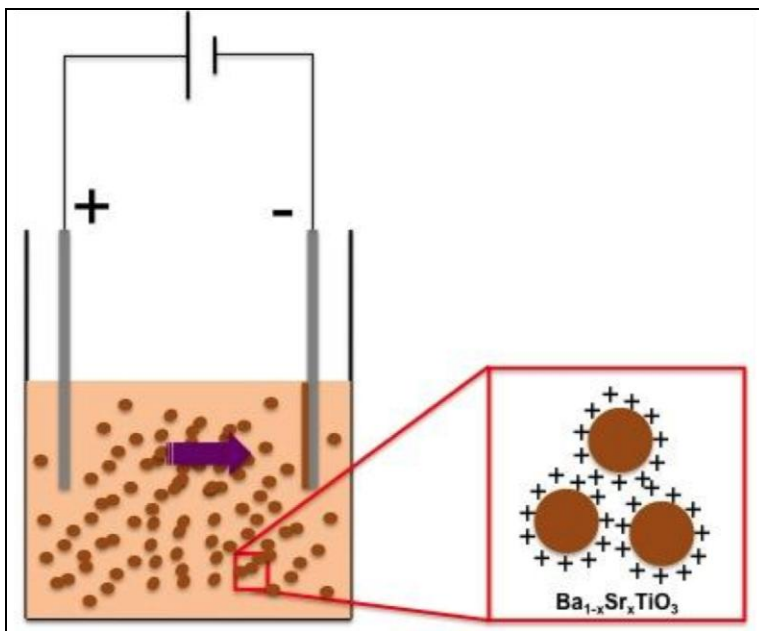


Figure 5. Schematic representation of EPD to fabricate  $\text{Ba}_{1-x}\text{Sr}_x\text{TiO}_3$  films.

Preliminary results using nickel (Ni) wires as electrodes,  $\text{Ba}_{1-x}\text{Sr}_x\text{TiO}_3$  nanoparticles suspended in methoxyethanol/AcAc at 3.3 g/L and deposition at 30 V produced the films deposited as a function of time as shown in figure 5. We observe that the thickness and quality of the resulting films are highly dependent on deposition time. Thicker films (up to  $\sim 10\ \mu\text{m}$ ) were produced by deposition for 30 min, but this extended time introduced extensive cracking; thinner films with significantly less cracking were produced by deposition for shorter times.

These preliminary results suggest that we will be able to optimize deposition parameters to produce ceria-doped  $\text{Ba}_{1-x}\text{Sr}_x\text{TiO}_3$  films with sufficiently uniform density to avoid the electrical shorting found by ARL in our spin-cast films, and with sufficient mechanical stability to survive the requisite processing and packaging steps.



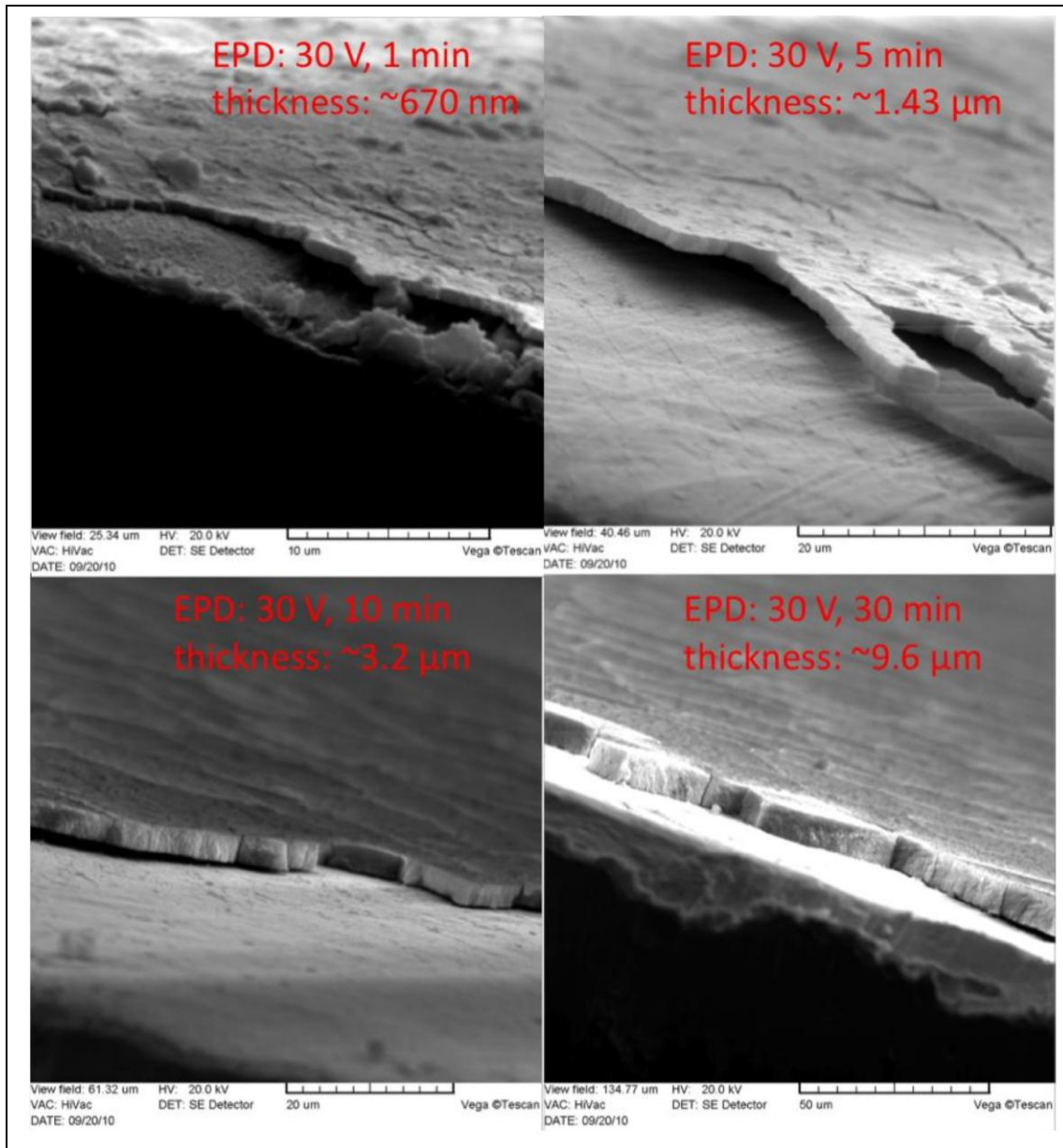


Figure 6. Scanning electron microscopy (SEM) images of films of  $\text{Ba}_{1-x}\text{Sr}_x\text{TiO}_3$  titanate nanoparticles deposited through electrophoretic deposition (EPD).

## 4. Progress by the U.S. Army Research Laboratory (ARL)

### 4.1 Electrical Characterization of Perovskite Films; Refinement of Metallization Protocol; $\text{Ba}_{1-x}\text{Sr}_x\text{TiO}_3$ Film Hybridization

By the beginning of this quarter, we had processed numerous  $\text{BaTiO}_3$  and  $\text{Ba}_{1-x}\text{Sr}_x\text{TiO}_3$  test structures from ICB films for electrical characterization. We found a perplexing problem that



once electrical contacts were placed onto the metalized film, we measured a dead short. When we use a test probe on pre-metalized and wire-bonded films, we find that the films have the appropriate insulating properties. Sufficient care was taken to be sure that we were not penetrating the film with our contact layers, and the ICB films were definitely sufficiently thick that we did not expect the metal to be seeping through any extraneous pores in the film.

The material must be insulating for the pixels to be isolated. As insurance, we fabricated test structures out of materials with known capacitances and achieved the expected results. Therefore, we were confident that there was no issue with our measurement setup.

Figure 7 shows a wire-bonded film that appeared to be insulating when measured prior to metallization and wire bonding. After the metallization and wire-bonding state, the material was shorting. We are still experimenting with the metallization step, and have not yet optimized the metal layer thickness. There are issues related to the surface tension that affect the ability of the metal layer to adhere to the film. That, however, cannot be the source of the short because we are certain that the metal layer is sufficiently “trapped” under the wire bonds (unlike the exposed pads, where some of the metal has come off). Furthermore, weak metallization would make the material less likely, not more likely, to short.

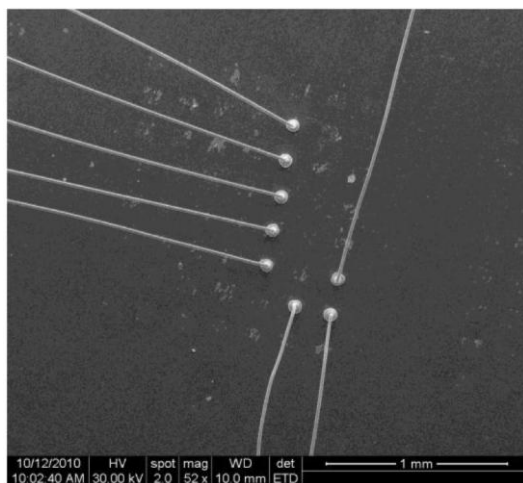


Figure 7.  $\text{Ba}_{1-x}\text{Sr}_x\text{TiO}_3$  thin-film following metallization and wire bonding.

Figure 8 shows a higher magnification image of a wire bond near the film. We were looking to see if the film had been punctured, indented, or damaged by the wire-bonding step. Damage from wire bonding was a problem when the films were softer, but SEM images show that the film is continuous and uncracked, and appears unaffected by the wire bonding.

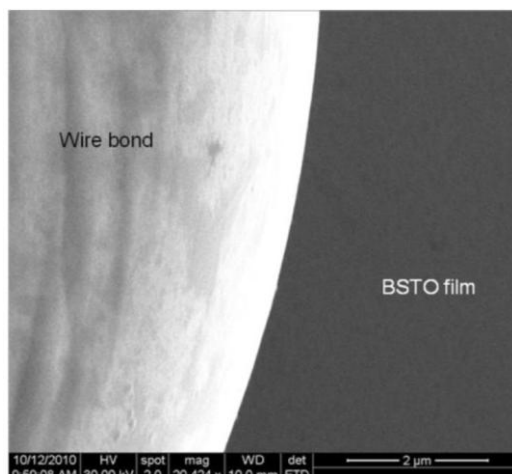


Figure 8. High magnification image of wire-bond  $\text{Ba}_{1-x}\text{Sr}_x\text{TiO}_3$  film interface.

The ICB provided us with abundant solution, made of 1.2 g of  $\text{Ba}_{1-x}\text{Sr}_x\text{TiO}_3$  nanoparticles suspended in 20 mL of hexane and 4.7 mL of oleic acid. The particles were precipitated with the addition of ethanol and redispersed in 20 mL of hexane only. After numerous trial-and-error attempts, we are currently using the following procedure: A silicon wafer was metalized in an electron beam evaporator with 300 Å of Ti followed by 1000 Å of Pt. The wafer was then diced into 1 cm<sup>2</sup> pieces. The  $\text{Ba}_{1-x}\text{Sr}_x\text{TiO}_3$  solution was filtered through a 0.2-μm filter using a 5-ml disposable syringe. The resulting fluid was spin-coated onto a Pt-coated silicon square at spin speeds of 1850 rpm/20 s followed by 2000 rpm/10 s. This spinning technique involved dropping three drops onto the center of the already spinning silicon. The  $\text{Ba}_{1-x}\text{Sr}_x\text{TiO}_3$ -coated silicon square was then hotplate baked at 340 °C for 10 min. This procedure was repeated for a total of three times. The coated silicon square was placed into a quartz tube furnace and baked at 600 °C for 1 h in an oxygen atmosphere. The film was cooled in the furnace to room temperature before removing. The resulting film thickness was approximately 400–500 nm.

Figure 9 shows an optimized  $\text{Ba}_{1-x}\text{Sr}_x\text{TiO}_3$  film that has been metalized and is ready for hybridization. Notice that the metal pad appears to be much improved compared with earlier versions (cf., figure 7). We are working to further optimize the metallization step. An indium bump was placed in the middle of the pad.

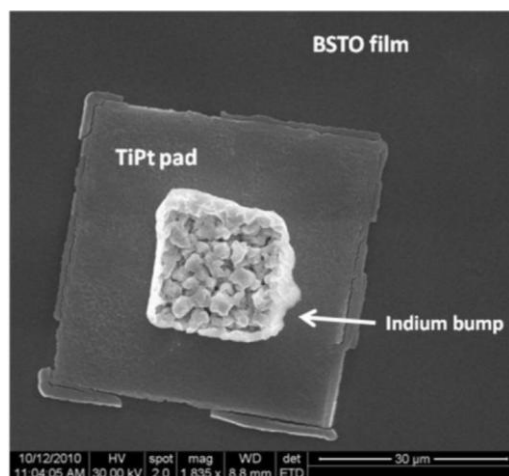


Figure 9. Optimized  $\text{Ba}_{1-x}\text{Sr}_x\text{TiO}_3$  thin film following metallization and prior to hybridization.

The sample was then hybridized as described elsewhere<sup>1</sup>. Briefly, flip-chip hybridization is a microelectronics packaging and assembly process, which directly connects an individual chip (device) to a substrate (readout) facedown, eliminating the need for peripheral wire bonding. Conductive connections are made between the two parts using interconnect bumps consisting of a solder material. Both parts are placed into a flip-chip hybrid bonder and, using thermo-compression as the bonding technique, “flipped” together. Flip-chip assembly is also known as direct chip attach (DCA), because the chip is directly attached to the substrate via conductive bumps. Flip-chip hybridization allows for lower lead resistance due to very short conductive bonds, and is a very reliable and robust technique due to the solder joint connections. It is capable of high density connections with a very low profile.

Preliminary measurements indicate that the hybridized sample made of the optimized  $\text{Ba}_{1-x}\text{Sr}_x\text{TiO}_3$  is electrically resistive. To be sure that the indium bumps were indeed making contact once the sample was hybridized, we pulled the sample apart and verified that the indium bumps had been “squished.” Figure 10 shows the sample after it has been pulled apart. The right side image is the fanout chip and the left side image is the  $\text{Ba}_{1-x}\text{Sr}_x\text{TiO}_3$  film. Notice that the indium bump on the  $\text{Ba}_{1-x}\text{Sr}_x\text{TiO}_3$  film is indeed squashed, with most of it now remaining on the fanout chip. Also notice the damage to the metallization layer, which again shows that we need to optimize the metallization. We did verify, however, that the metal remained intact under the indium bump.

We will now produce thicker films, as well as some films on quartz, that will be sent to Aerospace so that the relevant optical properties can be determined. The most recent batch of  $\text{Ba}_{1-x}\text{Sr}_x\text{TiO}_3$  films were sent to both Aerospace and the ICB.

<sup>1</sup>Olver, K. A. *Flip Chip Hybridization Using Indium Bump Technology at ARL*; ARL-TN-0283; U.S. Army Research Laboratory: Adelphi, MD, April 2007.

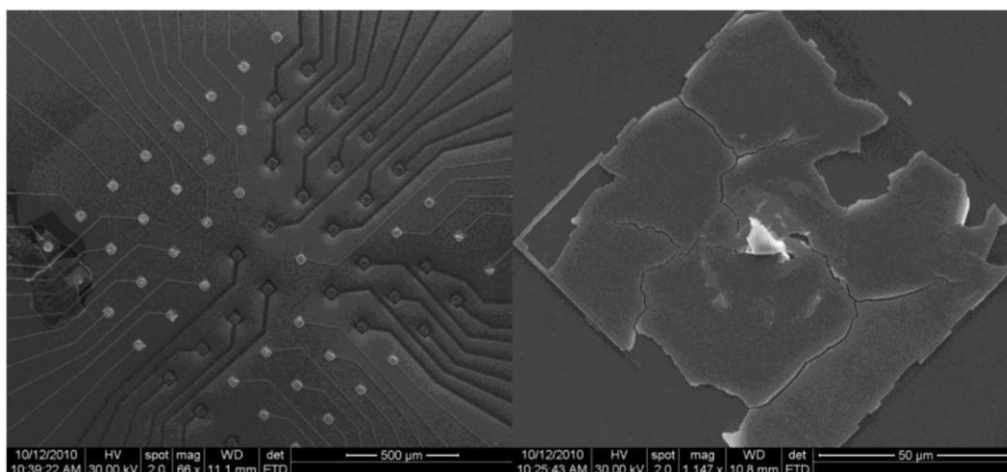


Figure 10. Hybridized  $\text{Ba}_{1-x}\text{Sr}_x\text{TiO}_3$  thin-film sample that has been pulled apart to verify proper indium bump contact. Images correspond to the film (left) and fanout chip (right).

## 5. Plans and Goals for Year 3, Quarter 2

In the coming quarter, we will continue to expand our nanomaterial synthesis capabilities; laser processing techniques and pyroelectric phase conversion studies; and perovskite thin-film electrical characterization efforts. We also intend to initiate and pursue several new areas of focus:

- *ICB*: Continue to develop and refine new electrophoretic nanoparticle deposition methods with particular emphasis on optimizing particle concentration, deposition time, and applied voltage parameters; further investigate the in-situ stabilization of perovskite nanoparticles using polyvinylpyrrolidone (PVP); and continue to provide perovskite nanoparticle films to Aerospace and ARL for laser-scripted pixelation/pyroelectric activation studies and electrical characterization of thin-film test structures.
- *Aerospace*: Continue fabrication of laser-pixelated perovskite thin-film array test structures for electrical analysis and IR responsiveness measurements by ARL; measure local PFM hysteresis curves for unexposed and laser-processed perovskite thin films to extract piezoelectric constants and assess intrinsic/residual stresses in the IR test structures; and explore the laser-induced annealing of the perovskite structures for improved film densification and electrical isolation.
- *ARL*: Continue to optimize the metallization protocol with particular attention on the influence of metal layer thickness on contact layer adhesion; further refine the hybridization techniques to facilitate the electrical characterization studies; and investigate the preparation of thicker micron-sized  $\text{Ba}_{1-x}\text{Sr}_x\text{TiO}_3$  films.

---

## List of Symbols, Abbreviations, and Acronyms

---

2-D	two-dimensional
AcAc	acetylacetone
AFM	atomic force microscopy
ARL	U.S. Army Research Laboratory
Ba <sub>1-x</sub> Sr <sub>x</sub> TiO <sub>3</sub>	barium strontium titanate
BaTiO <sub>3</sub>	barium titanium oxide
CeO <sub>2</sub>	cerium oxide
DCA	direct chip attach
DVE	driver vision enhancement
EPD	electrophoretic deposition
FPA	focal-plane array
FWHM	full width at half maximum
ICB	Institute for Collaborative Biotechnologies
IR	infrared
IR&D	Independent Research and Development
MEMS	microelectromechanical system
MOSD	metal-organic solution deposition
Ni	nickel
PDP	Product and Development Program
PFM	piezoelectric force microscopy
PVP	polyvinylpyrrolidone
RMS	root mean square
ROIC	readout integrated circuit
SEM	scanning electron microscopy

Si	silicon
SiO <sub>2</sub>	silicon dioxide
Ti/Pt	titanium platinum
UAVs	unattended aerial vehicles
UGSs	unattended ground sensors
UGVs	unmanned ground vehicles
Y3Q1	year three, quarter one

NO. OF COPIES	ORGANIZATION	NO. OF COPIES	ORGANIZATION
1 ELEC	ADMNSTR DEFNS TECHL INFO CTR ATTN DTIC OCP 8725 JOHN J KINGMAN RD STE 0944 FT BELVOIR VA 22060-6218	4	US ARMY RSRCH LAB ATTN IMNE ALC HRR MAIL & RECORDS MGMT ATTN RDRL CIO LL TECHL LIB ATTN RDRL CIO LT TECHL PUB ATTN RDRL SEE I W SARNEY ADELPHI MD 20783-1197
1	US ARMY RSRCH DEV AND ENGRG CMND ARMAMENT RSRCH DEV & ENGRG CTR ARMAMENT ENGRG & TECHNLOGY CTR ATTN AMSRD AAR AEF T J MATTS BLDG 305 ABERDEEN PROVING GROUND MD 21005-5001	TOTAL: 11 (1 ELEC, 10 HCS)	
1	US ARMY INFO SYS ENGRG CMND ATTN AMSEL IE TD A RIVERA FT HUACHUCA AZ 85613-5300		
1	US GOVERNMENT PRINT OFF DEPOSITORY RECEIVING SECTION ATTN MAIL STOP IDAD J TATE 732 NORTH CAPITOL ST NW WASHINGTON DC 20402		
2	INSTITUTE FOR COLLABORATIVE BIOTECHNOLOGIES UNIVERSITY OF CALIFORNIA, SANTA BARBARA ATTN D MORSE ATTN K NIESZ SANTA BARBARA CA 93106-5100		
1	THE AEROSPACE CORPORATION MICRO/NANOTECHNOLOGY DEPARTMENT SPACE MATERIALS LABORATORY ATTN F LIVINGSTON 2350 E EL SEGUNDO BLVD EL SEGUNDO CA 90245		

INTENTIONALLY LEFT BLANK.